Strongly nonlinear theory of rapid solidification near absolute stability

Katarzyna N. Kowal,* Anthony L. Altieri, and Stephen H. Davis
Department of Engineering Sciences and Applied Mathematics, Northwestern University, 2145 Sheridan Road, Evanston, Illinois 60208, USA
(Received 4 August 2017; published 9 October 2017)

We investigate the nonlinear evolution of the morphological deformation of a solid-liquid interface of a binary melt under rapid solidification conditions near two absolute stability limits. The first of these involves the complete stabilization of the system to cellular instabilities as a result of large enough surface energy. We derive nonlinear evolution equations in several limits in this scenario and investigate the effect of interfacial disequilibrium on the nonlinear deformations that arise. In contrast to the morphological stability problem in equilibrium, in which only cellular instabilities appear and only one absolute stability boundary exists, in disequilibrium the system is prone to oscillatory instabilities and a second absolute stability boundary involving attachment kinetics arises. Large enough attachment kinetics stabilize the oscillatory instabilities. We derive a nonlinear evolution equation to describe the nonlinear development of the solid-liquid interface near this oscillatory absolute stability limit. We find that strong asymmetries develop with time. For uniform oscillations, the evolution equation for the interface reduces to the simple form $f'' + (\beta f')^2 + f = 0$, where β is the disequilibrium parameter. Lastly, we investigate a distinguished limit near both absolute stability limits in which the system is prone to both cellular and oscillatory instabilities and derive a nonlinear evolution equation that captures the nonlinear deformations in this limit. Common to all these scenarios is the emergence of larger asymmetries in the resulting shapes of the solid-liquid interface with greater departures from equilibrium and larger morphological numbers. The disturbances additionally sharpen near the oscillatory absolute stability boundary, where the interface becomes deep-rooted. The oscillations are time-periodic only for small-enough initial amplitudes and their frequency depends on a single combination of physical parameters, including the morphological number, as well as the amplitude. The critical amplitude, at which solutions loose periodicity, depends on a single combination of parameters independent of the morphological number that indicate that non-periodic growth is most commonly present for moderate disequilibrium parameters. The spatial distribution of the interface develops deepening roots at late times. Similar spatial distributions are also seen in the limit in which both the cellular and oscillatory modes are close to absolute stability, and the roots deepen with larger departures from the two absolute stability boundaries.

DOI: 10.1103/PhysRevE.96.042801

I. INTRODUCTION

The directional solidification of binary alloys involves an interface between a solid and a liquid, which may become unstable. The mechanism of instability has been explained using linear stability theory by Mullins and Sekerka [1]. Coriell and McFadden [2] provide many generalizations of the model, which they have analyzed. The first weakly nonlinear theory of the development of the disturbances was developed by Wollkind and Segel [3]. It has been found that this instability can be suppressed if the surface energy is large enough, and the neighborhood of the critical value of the surface energy is referred to as a region of absolute stability. Brattkus and Davis [4] derived a strongly nonlinear evolution equation that describes the nonlinear dynamics of cellular modes in a neighborhood of the absolute stability boundary. These works involve systems at interfacial thermodynamic equilibrium.

For large solidification rates, the interface is no longer at thermodynamic equilibrium and one has to introduce generalizations to the phase diagram. Thermodynamically consistent generalizations have been developed by Baker and Cahn [5]; Jackson *et al.* [6]; Aziz [7]; Boettinger and Perepezko [8]; Boettinger and Coriell [9]; Kurz and Fisher [10] to include departures from equilibrium such as kinetic undercooling and solute trapping, which become important at high solidification rates. Coriell and Sekerka [11] used these generalizations in a linear stability theory model of interfacial disequilibrium and found that oscillatory instabilities may occur under rapid solidification conditions. Merchant and Davis [12] documented the whole state diagram for both modes—the cellular and the oscillatory modes. The latter are present only under interfacial disequilibrium. It has also been found that there is an absolute stability boundary for the oscillatory mode when attachment kinetics are taken to be large enough.

These works involve the linearised theory of systems exhibiting interfacial disequilibrium. A weakly nonlinear bifurcation analysis for the oscillatory mode under disequilibrium has been carried out by Braun and Davis [13], while a strongly nonlinear analysis of the oscillatory mode in the limit of small and large departure from equilibrium solute rejection has been conducted by Merchant *et al.* [14]. The weakly nonlinear interaction between the oscillatory and the cellular modes near their simultaneous onset has been examined by Braun *et al.* [15].

It is the purpose of the present paper to investigate the effect of disequilibrium on the nonlinear evolution of the solid-liquid interface near the cellular absolute stability boundary and the nonlinear development of long waves near the oscillatory absolute stability boundary for any level of disequilibrium.

*katarzyna.kowal@northwestern.edu

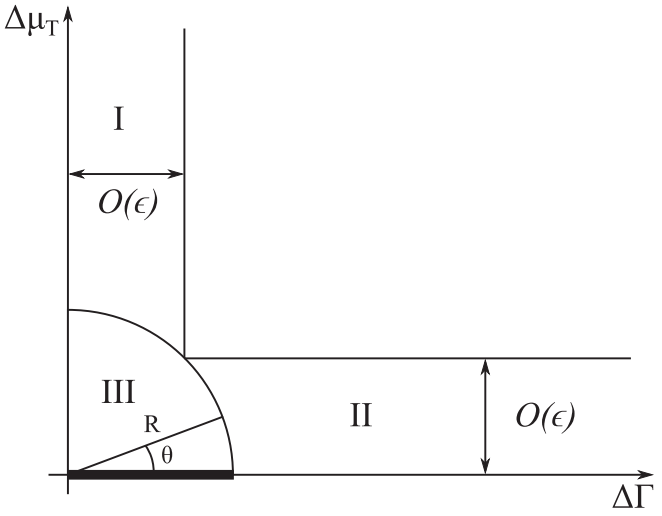

FIG. 1. Regime diagram in $(\Delta\Gamma, \Delta\mu_T)$ space, where $\Delta\Gamma = \Gamma_s - \Gamma$ and $\Delta\mu_T = \mu_{TS} - \mu_T$.

There are several limits that arise and we treat these separately, depending on the values of the surface energy Γ and attachment kinetics μ_T parameters and their closeness to their critical values Γ_s and μ_{TS}. A regime diagram depicting regions of parameter space close to the critical values is depicted in Fig. 1. The dynamics are intricately determined by the close interplay between the two absolute stability boundaries displayed in Fig. 1.

The first of these regimes, Regime I, is one in which $\Gamma - \Gamma_s = \mathcal{O}(\epsilon)$ and $\mu_T - \mu_{TS} = \mathcal{O}(1)$ as $\epsilon \to 0$, involving cellular growth near the cellular absolute stability boundary. The dynamics near absolute stability in this regime are dominated by the departure from critical attachment kinetics, specifically, by whether or not the system admits oscillatory instabilities. The larger the influence of disequilibrium and attachment kinetics, the deeper are the deformations and the larger are the asymmetries between root and tip regions. Similar behavior is seen as the morphological number increases.

Regime II involves the region of parameter space that is close to the oscillatory absolute stability boundary. Specifically, $\Gamma - \Gamma_s = \mathcal{O}(1)$ and $\mu_T - \mu_{TS} = \mathcal{O}(\epsilon)$ as $\epsilon \to 0$. This regime has been been studied in the limits of small and large disequilibrium parameter by Merchant *et al.* [14]. For general disequilibrium parameters in this regime, we find that the dynamics involves both periodic oscillations and monotonic growth, depending on the level of disequilibrium and the initial amplitude. In the limit of zero disequilibrium, all solutions are periodic in time for all amplitudes. Solutions are periodic in time only for small enough amplitudes once the disequilibrium parameter β is nonzero. Small amplitudes lead to near-sinusoidal solutions, which become more sharply rooted as the amplitude increases. Uniform oscillations are simply governed by the reduced evolution equation $f'' + (\beta f')^2 + f = 0$, where f is a scaled interfacial position. The frequency of the oscillations depends on the amplitude as well as on a single combination of physical parameters, including the morphological number. Once the initial amplitude exceeds a critical value, the solutions become non-periodic in time. The critical amplitude depends on a single combination of parameters and is smallest for $\beta = \mathcal{O}(1)$, and grows unboundedly for $\beta \to 0$ and $\beta \to \infty$. Non-periodic behavior in time is, therefore, most frequently present for $\beta = \mathcal{O}(1)$. The value of the morphological number influences only the period of the oscillations; it does not affect the critical amplitude. The spatial distribution of the disturbances develops strong asymmetries and sharply deepening troughs with time. Amplitudes near the troughs grow faster than near the peaks, leading to the strong asymmetry that develops with time.

Regime III is one in which both the cellular and oscillatory modes are close to absolute stability. We first derive an evolution equation for the amplitude when $\mu_T = \mu_{TS}$ and Γ close to Γ_s (depicted as the bold line in the figure), and then extend it to a distinguished limit in which both $\mu_{TS} - \mu_T$ and $\Gamma_s - \Gamma$ are small and nonzero. The dynamics are qualitatively similar to those of Brattkus and Davis [4], and reduce to Brattkus and Davis [4] in the limit of zero disequilibrium and zero attachment kinetics. Disequilibrium, departures from the two absolute stability boundaries, as well as increasing morphological numbers are seen to more strongly break symmetry and result in deepening roots in the resulting disturbances to the solid-liquid interface.

In each of these scenarios, we derive nonlinear evolution equations and solve them numerically. A common characteristic among all scenarios involves the appearance of stronger asymmetries with increasing disequilibrium and morphological numbers.

We begin by introducing the governing equations in Sec. II, we discuss the linear stability theory in Sec. III, and discuss the two absolute stability boundaries in Sec. IV. We then proceed by performing nonlinear stability analyses for cellular growth away from the oscillatory absolute stability boundary in Sec. V A, for cellular growth at critical attachment kinetics in Sec. V B, for oscillatory growth away from the cellular absolute stability boundary in Sec. VI, and for a distinguished limit near both of the absolute stability boundaries in Sec. VII. We finalize with conclusions in Sec. VIII.

II. THEORETICAL DEVELOPMENT

We consider the directional solidification of a dilute binary alloy under rapid solidification rates. Assumptions of local equilibrium at the solid-liquid interface no longer hold for large pulling speeds and disequilibrium effects such as kinetic undercooling and solute trapping become important. Departures from equilibrium result in alterations to the local interfacial temperature and solute concentrations derived from the phase diagram. These departures are formulated in the non-equilibrium model developed by Baker and Cahn [5]; Boettinger and Perepezko [8]; Boettinger and Coriell [9]; Kurz and Fisher [10].

We consider an infinite one-sided model, in the sense that the solute diffusivity in the solid phase is much smaller than that of the liquid phase. We adopt the frozen temperature approximation and assume that the solid and liquid phases have equal thermal properties, that the effects of latent heat are negligible.

We nondimensionalize the governing model based on solute diffusion so that the spatial and temporal variables as well as the solutal and temperature fields scale

as

$$\tilde{\boldsymbol{x}} = \frac{\mathcal{D}}{V}\boldsymbol{x}, \quad \tilde{t} = \frac{\mathcal{D}}{V^2}t, \tag{1a,b}$$

$$C = \frac{\tilde{C} - C_\infty/k_E}{C_\infty(k_E-1)/k_E}, \quad T = \frac{\tilde{T} - T_0}{G\mathcal{D}/V} \tag{2a,b}$$

(the quantities denoted by tildes are dimensional). We also nondimensionalize the normal velocity as

$$V_n = \tilde{V}_n/V. \tag{3}$$

Here, $\mathcal{D}$ is the solute diffusivity in the liquid, V is the pulling speed, C_∞ is the far-field solute concentration, T_0 is a reference temperature, G is the imposed thermal gradient, and k_E is the equilibrium segregation coefficient. The dimensionless parameters that appear are the surface energy Γ, the attachment kinetics parameter μ_T, the disequilibrium parameter β, and the morphological number $\mathcal{M}$. Explicitly,

$$\Gamma = \frac{T_M\tilde{\gamma}Vk_E}{L_v\mathcal{D}m_E(k_E-1)C_\infty}, \tag{4}$$

$$\mu_T = \frac{Vk_E}{(k_E-1)^2C_\infty V_0}, \tag{5}$$

$$\beta = \beta_0 V, \quad \mathcal{M} = \frac{m_E(k_E-1)C_\infty V}{\mathcal{D}Gk_E}, \tag{6a,b}$$

where T_M is the equilibrium melting temperature of the pure material, $\tilde{\gamma}$ is the surface energy, L_v is the latent heat per unit volume, and m_E is the equilibrium liquidus slope.

The local solute concentration satisfies

$$\frac{\partial C}{\partial t} - \frac{\partial C}{\partial z} = \nabla^2 C, \tag{7}$$

and is subject to the boundary conditions

$$T = \mathcal{M}\left[m(V_n)\left(C - \frac{1}{1-k_E}\right) + \frac{1}{1-k_E}\right] + 2H\mathcal{M}\Gamma - \mathcal{M}\mu_T V_n, \tag{8}$$

$$\left[C(1-k(V_n)) - \frac{1}{1+\beta V_n}\right]V_n = \left(\frac{\partial C}{\partial x}\frac{\partial h}{\partial x} + \frac{\partial C}{\partial y}\frac{\partial h}{\partial y} - \frac{\partial C}{\partial z}\right)(1+|\nabla h|^2)^{-1/2}, \tag{9}$$

at $z = h$ and the far field condition

$$C \to 1 \quad \text{as} \quad z \to \infty. \tag{10}$$

The first of these boundary conditions is the Gibbs-Thomson relation modified to incorporate kinetic undercooling, which may be important at large speeds (see, e.g., Merchant and Davis [12] and Davis [16]). The second of these reflects a local solute balance at the solid-liquid interface. In disequilibrium, the dimensionless segregation coefficient varies with the pulling speed and is given by

$$k(V_n) = \frac{k_E + \beta V_n}{1+\beta V_n}, \tag{11}$$

in the disequilibrium model proposed by Jackson *et al.* [6] and Aziz [7]. The segregation coefficient approaches unity at high pulling speeds, in which case solute becomes trapped into the solid. At low pulling speeds, the segregation coefficient approaches its equilibrium value k_E. For consistency, it is necessary for the change in liquidus slope to vary in V_n, via the segregation coefficient (see Baker and Cahn [5]; Boettinger and Perepezko [8]; Boettinger and Coriell [9]). A thermodynamically consistent expression for the dimensionless change in liquidus slope as a result of non-equilibrium segregation is given by

$$m(\tilde{V}_n) = m_E\left\{1 - \frac{1}{k_E-1}\left(k_E - k(V_n)\left[1 - \ln\frac{k(V_n)}{k_E}\right]\right)\right\} \tag{12}$$

(see Boettinger and Perepezko [8] and Boettinger and Coriell [9]).

Noting that the temperature is permanently of the form

$$T = z + \mathcal{M}\gamma, \tag{13}$$

where

$$\gamma = -\frac{k_E}{(1-k_E)^2}\mathcal{L} + \frac{\beta}{(1-k_E)(\beta+k_E)} - \mu_T, \tag{14}$$

and

$$\mathcal{L} = \ln(\bar{k}/k_E), \quad \bar{k} = \frac{k_E+\beta}{1+\beta}, \tag{15a,b}$$

we note that boundary condition (8) reduces to

$$h + \mathcal{M}\gamma = \mathcal{M}\left[m(V_n)\left(C - \frac{1}{1-k_E}\right) + \frac{1}{1-k_E}\right] + 2H\mathcal{M}\Gamma - \mathcal{M}\mu_T V_n \tag{16}$$

involving the solutal field and position of the solid-liquid interface.

III. BASIC STATE AND LINEAR STABILITY

The basic state is given by a planar interface and exponential solutal field

$$h_0 = 0, \; C_0 = 1 - \delta e^{-z}, \tag{17a,b}$$

where $\delta = k_E/(k_E+\beta)$. Perturbing about this solution and searching for normal modes of the form

$$h = h_0 + \epsilon h_1 e^{i\boldsymbol{\alpha}\cdot\boldsymbol{x}+\sigma t}, \quad C = C_0(z) + \epsilon C_1(z) e^{i\boldsymbol{\alpha}\cdot\boldsymbol{x}+\sigma t}, \tag{18}$$

where

$$\boldsymbol{\alpha} = (\alpha_1, \alpha_2) \tag{19}$$

is the wave vector, $\alpha = |\boldsymbol{\alpha}|$ and $\boldsymbol{x} = (x, y)$, yields the characteristic equation

$$\mathcal{M}^{-1} = \frac{\delta(\mathcal{L}(\beta+k_E) + (1-k_E))}{(\beta+1)(1-k_E)} \cdot \left(1 - \frac{2(\beta+k_E+\sigma)}{(\beta+1)\lambda_1 + \beta + 2k_E - 1}\right) - \alpha^2\Gamma - \sigma\mu_T - \frac{\delta\beta\sigma\mathcal{L}}{(\beta+1)(1-k_E)}, \tag{20}$$

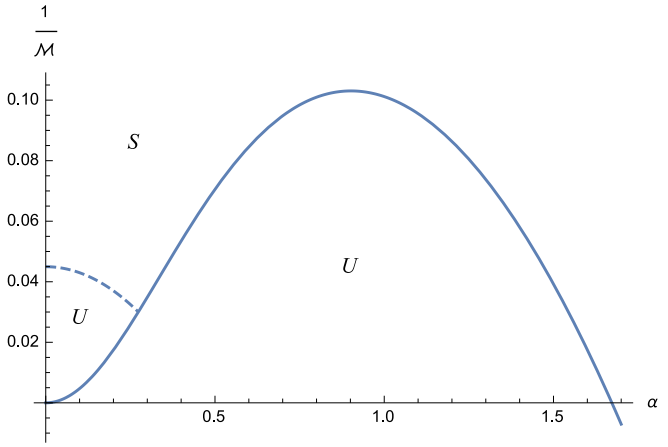

FIG. 2. Neutral stability curve, $\mathcal{M}^{-1}$ versus α. The solid curve denotes the cellular branch, whereas the dashed curve denotes the oscillatory branch.

derived by Merchant and Davis [12], where

$$\lambda_1 = \sqrt{4\alpha^2 + 4\sigma + 1}. \tag{21}$$

The neutral stability curve is presented in Fig. 2. Two types of instabilities emerge: cellular instabilities and oscillatory instabilities. In disequilibrium, the neutral stability curve is composed of two branches: a cellular branch and an oscillatory branch. These lead to two absolute stability boundaries, one in Γ and one in μ_T.

IV. ABSOLUTE STABILITY BOUNDARIES

The characteristic equation gives rise to a band of unstable wave numbers, with a finite-wave number cutoff at $\alpha = \alpha_s$ for the cellular mode. Disturbances with $\alpha > \alpha_s$ are stabilized by surface energy. The critical wave number $\alpha = \alpha_c$ that corresponds to the maximal inverse morphological number $\mathcal{M}_c^{-1}$ is shown in Fig. 3. For large enough surface energy Γ, the system is completely stable to cellular instabilities. Specifically, this occurs for $\Gamma > \Gamma_s$, where

$$\Gamma_s = k_E \frac{(1-k_E) + (k_E+\beta)\mathcal{L}}{(1-k_E)(\beta+k_E)^2} \tag{22}$$

as derived by Merchant and Davis [12]. The locus $\Gamma = \Gamma_s$ is one of the absolute stability boundaries inherent to the morphological stability problem in disequilibrium. The strongly nonlinear analysis of Brattkus and Davis [4] reveals the strongly nonlinear structure of the disturbances near this absolute stability boundary in interfacial equilibrium. We wish to generalize this to include the effects of disequilibrium, as well as to investigate the the nonlinear evolution of disturbances near the oscillatory absolute stability boundary, which appears only in disequilibrium.

The oscillatory absolute stability boundary involves attachment kinetics. For large enough kinetics parameter μ_T, the system is completely stable to oscillatory instabilities for all wave numbers. This occurs for $\mu_T > \mu_{TS}$, where

$$\mu_{TS} = \frac{\beta k_E}{(\beta+1)(\beta+k_E)^2} \tag{23}$$

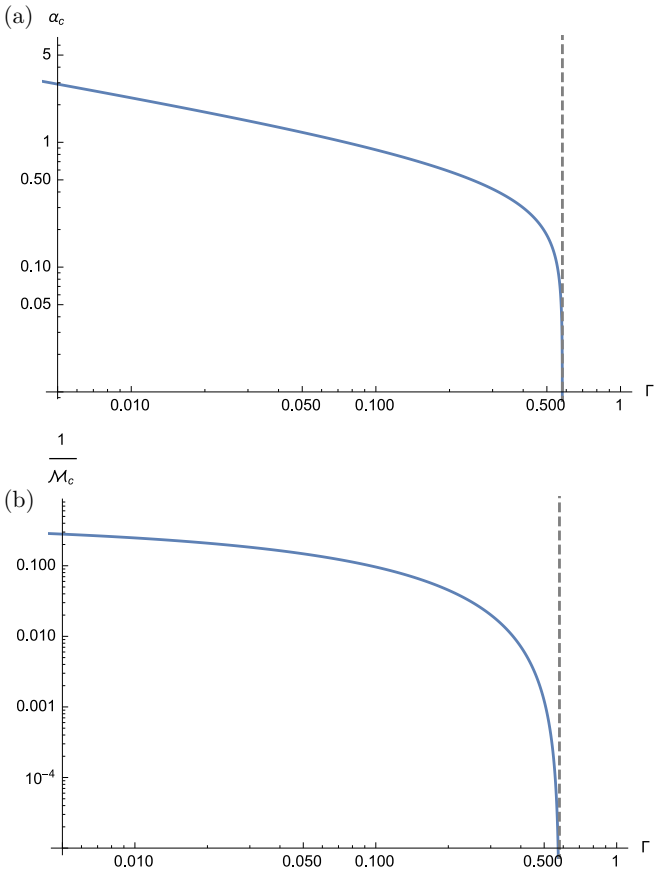

FIG. 3. Critical wave number α_c and $\mathcal{M}_c^{-1}$ as a function of Γ for the steady mode. The absolute stability boundary $\Gamma = \Gamma_s$ is shown as a dashed line.

(see Merchant and Davis [12]). Oscillatory instabilities are possible for $\mu_T < \mu_{TS}$ within a band of unstable wave numbers given by $\alpha < \alpha_{oc}$. A representative plot of α_{oc} and the corresponding inverse morphological number $\mathcal{M}_{oc}^{-1}$ as a function of the attachment kinetics parameter is shown in Fig. 4.

There are several different scenarios that may arise near the various absolute stability boundaries in parameter space. We begin by conducting a nonlinear analysis near the cellular absolute stability boundary $\Gamma = \Gamma_s$, which closely depends on μ_T. We divide our analysis into subsections, that depend on the closeness of μ_T to the oscillatory absolute stability boundary.

V. NONLINEAR CELLULAR GROWTH—REGIME I

A. Cellular growth away from critical attachment kinetics

In this section, we investigate the nonlinear evolution of the deformed solid-liquid interface near the cellular absolute stability boundary $\Gamma = \Gamma_s$, such that $\mu_T - \mu_{TS} = \mathcal{O}(1)$ as $\Gamma \to \Gamma_s$.

If we define the difference between Γ and Γ_s by a small parameter ϵ, then the appropriate scalings near the absolute cellular stability boundary for $\mu_T \neq \mu_{TS}$ are

$$\Gamma = \Gamma_s - \epsilon, \quad \alpha = \epsilon^{1/2}\bar{\alpha},$$
$$\sigma = \epsilon^2\bar{\sigma}, \quad \mathcal{M}^{-1} = \epsilon^2\bar{\mathcal{M}}^{-1}, \tag{24a–d}$$

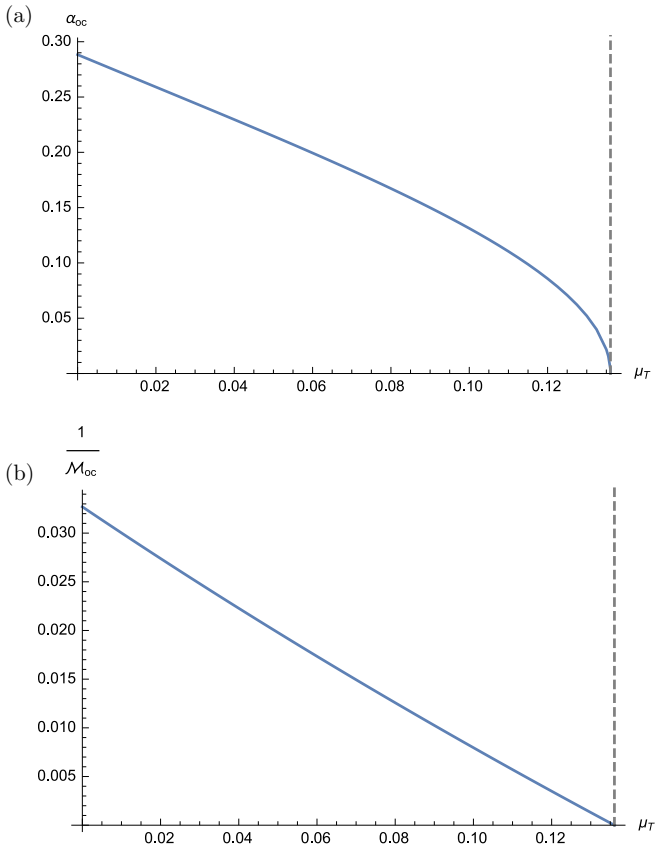

FIG. 4. Critical wave number α_{oc} and inverse morphological number $\mathcal{M}_{oc}^{-1}$ as a function of the attachment kinetics parameter. The absolute stability boundary $\mu_T = \mu_{TS}$ is shown as a dashed line.

under which, the dispersion relation becomes

$$\bar{\mathcal{M}}^{-1} = \bar{\alpha}^2 - \frac{\Gamma_s(2\beta + k_E + 1)}{\beta + k_E}\bar{\alpha}^4 + (\mu_{TS} - \mu_T)\bar{\sigma} \tag{25}$$

at leading order. The scaling is consistent with that used by Brattkus and Davis [4] apart from the scaling for σ, chosen in order to balance the effects of disequilibrium. Specifically, if σ is scaled as in [4], then there is an imbalance at order ϵ, unless μ_T is chosen to be exactly its critical value μ_{TS}. This special case ($\mu_T = \mu_{TS}$) is examined in Sec. V B and corresponds directly to the results of Brattkus and Davis [4].

To examine the nonlinear growth near this absolute stability boundary (where $\mu_T - \mu_{TS} = \mathcal{O}(1)$ as $\Gamma \to \Gamma_s$), we define

$$\tau = \epsilon^2 t, \quad (\xi,\eta) = \epsilon^{1/2}(x,y), \quad \zeta = z - h. \tag{26a–c}$$

The last substitution aids in applying boundary conditions at the deformed interface $z = h$. Under this transformation, the governing equations become

$$\epsilon^2\left(\frac{\partial C}{\partial \tau} - \frac{\partial h}{\partial \tau}\frac{\partial C}{\partial \zeta}\right) = \epsilon\left(\frac{\partial^2 C}{\partial \zeta^2}|\nabla(h)|^2 - 2\nabla h\cdot\frac{\partial \nabla C}{\partial \zeta} - \frac{\partial C}{\partial \zeta}\nabla^2 h + \nabla^2 C\right) + \frac{\partial^2 C}{\partial \zeta^2} + \frac{\partial C}{\partial \zeta} \tag{27}$$

for $\zeta > 0$, and

$$h\epsilon^2\bar{\mathcal{M}}^{-1} + \gamma = m\left(C + \frac{1}{k_E - 1}\right) + 2H(\Gamma_s - \epsilon) - \frac{1}{k_E - 1} - \mu_T V_n, \tag{28}$$

$$V_n\left(C(1-k) - \frac{1}{\beta V_n + 1}\right) = \frac{(\epsilon\nabla C - C_\zeta \nabla h)\cdot\nabla h - C_\zeta}{\sqrt{\epsilon\nabla h\cdot\nabla h + 1}} \tag{29}$$

at $\zeta = 0$, and

$$C \to 1 \quad \text{as} \quad \zeta \to \infty, \tag{30}$$

where the normal velocity and mean curvature are given by

$$V_n = \frac{1 + \epsilon^2 h_\tau}{\sqrt{1 + \epsilon|\nabla h|^2}} \tag{31}$$

and

$$\bar{H} = \left[\epsilon h_{\xi\xi}\left(1 + \epsilon h_\eta^2\right) - 2\epsilon^2 h_\eta h_\xi h_{\xi\eta} + \epsilon h_{\eta\eta}\left(1 + \epsilon h_\xi^2\right)\right]\cdot[1 + \epsilon|\nabla h|^2]^{-3/2}, \tag{32}$$

respectively.

We expand in the small parameter ϵ as follows

$$C = C_0 + \epsilon C_1 + \epsilon^2 C_2 + \cdots, \quad h = h_0 + \epsilon h_1 + \epsilon^2 h_2 + \cdots \tag{33}$$

with the normal velocity

$$V_n = V_0 + \epsilon V_1 + \epsilon^2 V_2 + \cdots, \tag{34}$$

and the mean curvature

$$2\bar{H} = 2\bar{H}_1\epsilon + 2\bar{H}_2\epsilon^2 + \cdots, \tag{35}$$

where

$$V_0 = 1, \quad V_1 = -\tfrac{1}{2}|\nabla h_0|^2, \quad V_2 = h_{0\tau} + \tfrac{3}{8}|\nabla h_0|^4 - \nabla h_0 \nabla h_1, \tag{35a–c}$$

and

$$2\bar{H}_1 = \nabla^2 h_0, \quad 2\bar{H}_2 = \nabla^2 h_1 - \tfrac{1}{2}|\nabla h_0|^2\nabla^2 h_0 - \tfrac{1}{2}\nabla h_0 \nabla|\nabla h_0|^2. \tag{36a,b}$$

The segregation coefficient becomes

$$k(V_n) = \frac{k_E + \beta V_n}{1 + \beta V_n} = k_0 + \epsilon k_1 + \epsilon^2 k_2 + \cdots, \tag{37}$$

where

$$k_0 = \frac{k_E + \beta}{1 + \beta}, \quad k_1 = \frac{(1 - k_E)\beta}{(1 + \beta)^2}V_1, \quad k_2 = \frac{(1 - k_E)\beta}{(1 + \beta)^3}\left((1 + \beta)V_2 - \beta V_1^2\right), \tag{38a–c}$$

and the liquidus slope becomes

$$m(V_n) = m_0 + \epsilon m_1 + \epsilon^2 m_2 + \cdots, \tag{39}$$

where

$$m_0 = \frac{k_0(1-\mathcal{L})-1}{k_E-1}, \tag{40}$$

$$m_1 = \frac{\mathcal{L}k_1}{1-k_E}, \tag{41}$$

$$m_2 = \frac{k_1^2+2\mathcal{L}k_0k_2}{2k_0(1-k_E)}. \tag{42}$$

1. Zeroth order

At zeroth order in ϵ, the system becomes

$$C_{0\zeta}+C_{0\zeta\zeta}=0, \tag{43}$$

subject to the boundary conditions

$$\gamma = C_0m_0+\frac{m_0}{k_E-1}-\frac{1}{k_E-1}-\mu_T \tag{44}$$

and

$$-\frac{1}{\beta+1}+C_0(1-k_0)=-C_{0\zeta} \tag{45}$$

at $\zeta=0$, and

$$C_0\to 1 \quad \text{as} \quad \zeta\to\infty. \tag{46}$$

The solution is

$$C_0 = 1-\delta e^{-\zeta}. \tag{47}$$

2. First order

At order ϵ, the system reduces to

$$C_{1\zeta}+C_{1\zeta\zeta} = \nabla^2h_0C_{0,\zeta}-C_{0\zeta\zeta}|\nabla h_0|^2 + 2\nabla h_0\cdot\nabla C_{0,\zeta}-\nabla^2C_0, \tag{48}$$

for $\zeta>0$, subject to

$$2\bar{H}_1\Gamma_s+C_1m_0+C_0m_1+\frac{m_1}{k_E-1}-\mu_TV_1=0, \tag{49}$$

and

$$-C_{1,\zeta}-\frac{1}{2}\delta|\nabla h_0|^2 = C_1(1-k_0)-(1-\delta)k_1 - V_1\left[(1-\delta)(k_0-1)+\tfrac{1}{(\beta+1)^2}\right], \tag{50}$$

at $\zeta=0$, and

$$C_1\to 0 \quad \text{as} \quad \zeta\to\infty. \tag{51}$$

Solutions exist only if

$$h_0 = \text{const} \quad \text{and} \quad C_1=0. \tag{52}$$

3. Second order

At order ϵ^2, the system reduces to

$$C_{2\zeta}+C_{2\zeta\zeta}=(\delta\nabla^2h_1)e^{-\zeta} \tag{53}$$

for $\zeta>0$, subject to

$$h_0\bar{\mathcal{M}}^{-1} = 2\bar{H}_2\Gamma_s-2\bar{H}_1+C_2m_0+C_1m_1 + C_0m_2+\frac{m_2}{k_E-1}-\mu_TV_2, \tag{54}$$

and

$$-C_{2\zeta} = C_2(1-k_0)-(1-\delta)k_2 - V_2\left((1-\delta)(k_0-1)+\frac{1}{(\beta+1)^2}\right), \tag{55}$$

at $\zeta=0$, and the decay condition

$$C_2\to 0 \quad \text{as} \quad \zeta\to\infty. \tag{56}$$

The solution is given by

$$C_2 = -\delta\left(\zeta+\frac{1}{k_0}\right)e^{-\zeta}\nabla^2h_1. \tag{57}$$

4. Third order

Finally, at order ϵ^3, the system reduces to

$$C_{3\zeta}+C_{3\zeta\zeta} = \delta e^{-\zeta}\nabla^2h_2+\delta e^{-\zeta}|\nabla h_1|^2 - \delta e^{-\zeta}h_{1\tau}-\nabla^2C_2, \tag{58}$$

for $\zeta>0$,

$$h_1\bar{\mathcal{M}}^{-1} = 2\bar{H}_3\Gamma_s-2\bar{H}_2+C_3m_0+C_2m_1 + C_1m_2+C_0k_3+\frac{k_3}{k_E-1}-\mu_TV_3, \tag{59}$$

and

$$-C_{3,\zeta}-\frac{1}{2}\delta|\nabla h_1|^2 = C_3(1-k_0)-(1-\delta)k_3 - \frac{V_3((\beta+1)^2(1-\delta)(k_0-1)+1)}{(\beta+1)^2}, \tag{60}$$

at $\zeta=0$, and

$$C_3\to 0 \quad \text{as} \quad \zeta\to\infty. \tag{61}$$

Solutions exist only if the system obeys the following orthogonality condition:

$$h_1\bar{\mathcal{M}}^{-1} = (\mu_T-\mu_{TS})\left(\frac{1}{2}|\nabla h_1|^2-\frac{\partial h_1}{\partial\tau}\right) - \nabla^2h_1-\left(2+\frac{1-k_E}{k_E+\beta}\right)\Gamma_s\nabla^4h_1. \tag{62}$$

This is an evolution for the cellular growth of the solid-liquid interface near absolute stability. In contrast to the long-wave evolution equation presented by Brattkus and Davis [4], here the departure from critical attachment kinetics is significant and determines the long-time dynamics. Spatially uniform disturbances grow exponentially if $\mu_T<\mu_{TS}$ and decay if $\mu_T>\mu_{TS}$. That is, the long-time behavior of uniform disturbances depends on whether the system admits oscillatory modes.

The steady, spatially independent version of this equation is given by

$$h_1\bar{\mathcal{M}}^{-1} = \frac{1}{2}(\mu_T-\mu_{TS})(h_1')^2-h_1'' - \left(2+\frac{1-k_E}{k_E+\beta}\right)\Gamma_sh_1'''', \tag{63}$$

the solution of which is shown in Fig. 5 for various values of β, $\bar{\mathcal{M}}$, and μ_T at the critical wavelength $\xi=\xi_a$. Here, we have

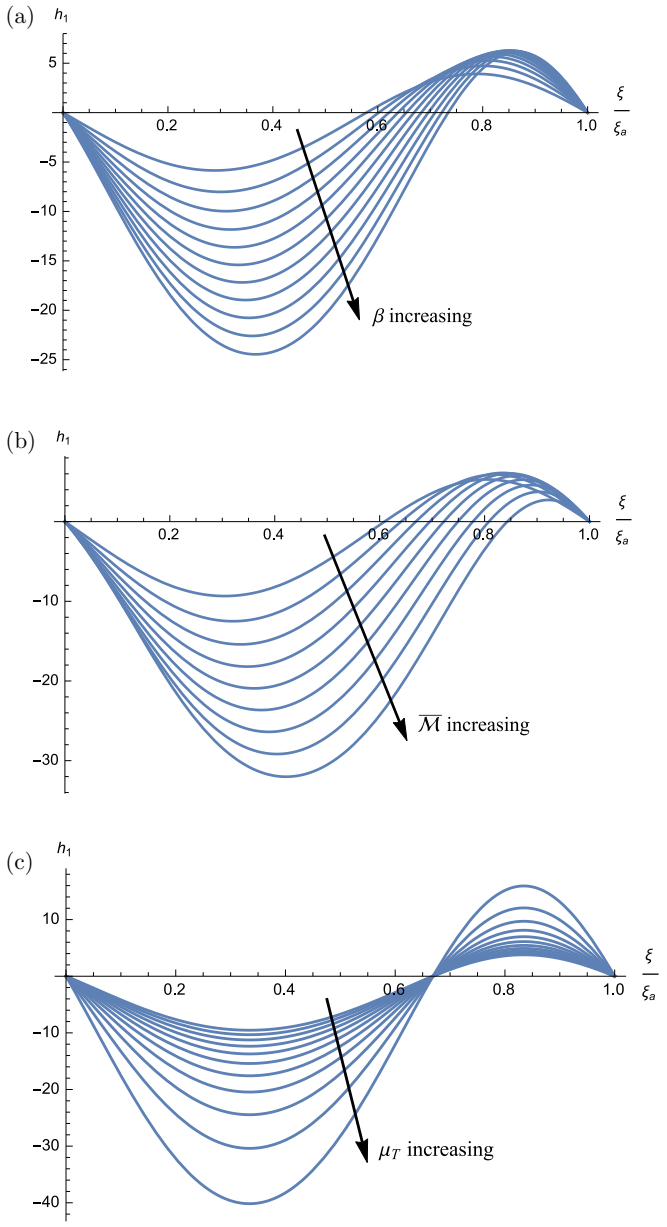

FIG. 5. The steady deformation of the solid-liquid interface in one horizontal dimension near the cellular absolute stability limit $\Gamma = \Gamma_s$, when μ_T is bounded away from its critical value μ_{TS}, for varying (a) β, (b) $\bar{\mathcal{M}}$, and (c) μ_T. The horizontal axis is normalized by the critical wavelength ξ_a (which varies as a function of the physical parameters) Here, $k_E = 0.8$, and $\Gamma = 1$. In (b) and (c), $\beta = 0.9$ is fixed. In (a) and (b) $\mu_T = 0.05$ is fixed. In (a) and (c), $\bar{\mathcal{M}} = 5$ is fixed.

imposed periodic boundary conditions. Large β, $\bar{\mathcal{M}}$, and μ_T give rise to deeper deformations and stronger asymmetries.

We note that unlike in equilibrium, the full time- and space-dependent evolution equation does not involve interfacial acceleration, which, instead, appears at higher orders because the effects of attachment kinetics are more significant, unless $|\mu_T - \mu_{TS}|$ is small. Second-order derivatives in time appear closer to the oscillatory absolute stability boundary, that is, in the special case when $\mu_T = \mu_{TS}$ and in a distinguished limit in which both $\Gamma - \Gamma_s$ and $\mu_T - \mu_{TS}$ are small. The evolution equation in the case in which $\mu_T = \mu_{TS}$, examined in Sec. V B, exhibits interfacial acceleration, and is more closely linked to the results of Brattkus and Davis [4]. Keeping this higher-order contribution results in the following modification to the evolution equation:

$$h_1\bar{\mathcal{M}}^{-1} = (\mu_T - \mu_{TS})\left(\frac{1}{2}|\nabla h_1|^2 - \frac{\partial h_1}{\partial \tau}\right) - \nabla^2 h_1 - \left(2 + \frac{1-k_E}{k_E+\beta}\right)\Gamma_s\nabla^4 h_1 - \epsilon^2\Gamma_s\frac{k_E+2\beta}{k_E+\beta}h_{1\tau\tau} + r(h_1,h_2,\epsilon), \tag{64}$$

where $r(h_1,h_2,\epsilon)$ is a residual function independent of $h_{1\tau\tau}$. The spatially uniform version of this equation for negligible r gives oscillatory solutions, indicating that the amplitude of the solutions h_1 evolves additionally on a slow time scale as a result of the oscillatory instabilities still present in this regime.

B. Cellular growth at critical attachment kinetics

When the attachment kinetics parameter reaches its critical value $\mu_T = \mu_{TS}$, the oscillatory instability no longer appears and there are fundamentally different dynamics of the cellular branch near absolute stability. In particular, the scalings

$$\Gamma = \Gamma_s - \epsilon, \quad \alpha = \epsilon^{1/2}\bar{\alpha}, \quad \sigma = \epsilon\bar{\sigma}, \quad \mathcal{M}^{-1} = \epsilon^2\bar{\mathcal{M}}^{-1}, \quad \mu_T = \mu_{TS}, \tag{64a–e}$$

used by Brattkus and Davis [4] are appropriate in this case. We define the transformation

$$\tau = \epsilon t, \quad (\xi,\eta) = \epsilon^{1/2}(x,y), \quad \zeta = z - h, \tag{65a–c}$$

under which the system reduces to

$$\epsilon(C_\tau - C_\zeta h_\tau) = \epsilon(C_{\zeta\zeta}|\nabla h|^2 - C_\zeta\nabla^2 h - 2\nabla h\nabla C_\zeta + \nabla^2 C) + C_\zeta + C_{\zeta\zeta}, \tag{66}$$

for $\zeta > 0$, subject to

$$\epsilon^2 h\bar{\mathcal{M}}^{-1} + \gamma = 2\bar{H}(\Gamma_s - \epsilon) - \mu_{TS}\bar{V}_n - \frac{1}{k_E - 1} + m\left(C + \frac{1}{k_E - 1}\right), \tag{67}$$

and

$$\left(C(1-k) - \frac{1}{\beta\bar{V}_n + 1}\right)\bar{V}_n = [\epsilon(\nabla C - C_\zeta\nabla h)\nabla h - C_\zeta][1 + \epsilon|\nabla h|^2]^{-1/2}, \tag{68}$$

at $\zeta = 0$, and

$$C \to 1 \quad \text{as} \quad \zeta \to \infty, \tag{69}$$

where

$$\bar{V}_n = \frac{\epsilon h_\tau + 1}{\sqrt{\epsilon|\nabla h|^2 + 1}}, \tag{70}$$

and

$$2\bar{H} = \big[\epsilon h_{\xi\xi}\big(\epsilon h_\eta^2 + 1\big) - 2\epsilon^2 h_\eta h_\xi h_{\xi\eta} + \epsilon h_{\eta\eta}\big(\epsilon h_\xi^2 + 1\big)\big][\epsilon|\nabla h|^2 + 1]^{-3/2}. \quad (71)$$

We expand in powers of ϵ as

$$C = C_0 + \epsilon C_1 + \epsilon^2 C_2 + \cdots, \quad h = h_0 + \epsilon h_1 + \epsilon^2 h_2 + \cdots. \quad (72a,b)$$

1. Zeroth order

At zeroth order in ϵ, the system reduces to

$$C_{0\zeta} + C_{0\zeta\zeta} = 0, \quad (73)$$

for $\zeta > 0$,

$$\gamma = C_0 m_0 + \frac{m_0}{k_E - 1} - \frac{1}{k_E - 1} - \mu_{TS}, \quad (74)$$

and

$$-\frac{1}{\beta + 1} + C_0(1 - k_0) = -C_{0\zeta}, \quad (75)$$

at $\zeta = 0$, and

$$C_0 \to 1 \quad \text{as} \quad \zeta \to \infty, \quad (76)$$

which has the solution

$$C_0 = 1 - \delta e^{-\zeta}, \quad (77)$$

as before.

2. First order

At first order in ϵ, the system reduces to

$$-\delta e^{-\zeta} h_{0\tau} = C_{1\zeta} + C_{1\zeta\zeta} - \delta e^{-\zeta}\nabla^2 h_0 - \delta e^{-\zeta}|\nabla h_0|^2, \quad (78)$$

for $\zeta > 0$,

$$0 = 2\bar{H}_1\Gamma_s + C_1 m_0 + C_0 m_1 + \frac{m_1}{k_E - 1} - V_1\mu_{TS}, \quad (79)$$

and

$$-C_{1\zeta} - \frac{1}{2}\delta|\nabla h_0|^2 = C_1(1 - k_0) - (1 - \delta)k_1 - V_1\left((1 - \delta)(k_0 - 1) + \frac{1}{(\beta + 1)^2}\right), \quad (80)$$

at $\zeta = 0$, and

$$C_1 \to 0 \quad \text{as} \quad \zeta \to \infty, \quad (81)$$

which has the solution

$$C_1 = e^{-\zeta}[a - \delta\zeta(-h_{0,\tau} + \nabla^2(h_0) + |\nabla h_0|^2)], \quad (82)$$

where

$$a = \frac{k_E}{2(\beta + k_E)^2}(2\beta h_{0\tau} - 2(\beta + 1)\nabla^2 h_0 - \beta|\nabla h_0|^2). \quad (83)$$

3. Second order

At second order in ϵ, the system reduces to

$$\begin{aligned} &- C_{1\zeta}h_{0\tau} - C_{0\zeta}h_{1\tau} + C_{1\tau} \\ &\quad = C_{2\zeta} + C_{2\zeta\zeta} - C_{1\zeta}\nabla^2 h_0 \\ &\qquad - C_{0\zeta}\nabla^2 h_1 + C_{1\zeta\zeta}|\nabla h_0|^2 - 2\nabla h_0 \cdot \nabla C_{1\zeta} \\ &\qquad - 2\nabla h_1 \cdot \nabla C_{0\zeta} + 2C_{0\zeta\zeta}\nabla h_0 \cdot \nabla h_1 + \nabla^2 C_1, \end{aligned} \quad (84)$$

for $\zeta > 0$,

$$h_0\bar{\mathcal{M}}^{-1} = 2\bar{H}_2\Gamma_s - 2\bar{H}_1 + a m_1 - \frac{b m_0}{2} + \frac{m_2}{k_E - 1} + (1 - \delta)m_2 - V_2\mu_{TS}, \quad (85)$$

and

$$\begin{aligned} &- C_0 k_2 - V_2\left(C_0(k_0 - 1) + \frac{1}{(\beta + 1)^2}\right) + C_2(1 - k_0) \\ &- C_1 k_1 + V_1(C_1(1 - k_0) - C_0 k_1) + \frac{\beta V_1^2}{(\beta + 1)^3} \\ &\quad = \frac{1}{2}|\nabla h_0|^2(C_{1,\xi} - \nabla h_0 \cdot \nabla(C_0 - h_0 C_{0,\xi})) \\ &\qquad - C_{2,\xi} + \nabla h_1 \cdot \nabla(C_0 - h_0 C_{0,\xi}) \\ &\qquad + \nabla h_0 \cdot \nabla(C_1 - h_0 C_{1,\xi} - h_1 C_{0,\xi}) \\ &\qquad + C_{0,\xi}\left(\nabla h_0 \cdot \nabla h_1 - \frac{3}{8}|\nabla h_0|^4\right), \end{aligned} \quad (86)$$

at $\zeta = 0$, and

$$C_2 \to 0 \quad \text{as} \quad \zeta \to \infty. \quad (87)$$

Solutions exist only when the amplitude h_0 satisfies the following evolution equation:

$$\begin{aligned} h_0\bar{\mathcal{M}}^{-1}(k_E + \beta) = &- (1 + \beta)\Gamma_s \nabla h_0 \cdot \nabla(\nabla^2 h_0) - \left(\frac{1}{2}k_E + \beta\right)\Gamma_s \nabla h_0 \cdot \nabla(|\nabla h_0|^2) + \frac{\mu_{TS}\beta(2 + k_E + 3\beta)}{2(1 + \beta)}\frac{\partial h_0}{\partial \tau}|\nabla h_0|^2 \\ &- \frac{\mu_{TS}\beta(2 + k_E + 3\beta)}{2(1 + \beta)}\left(\frac{\partial h_0}{\partial \tau}\right)^2 - (k_E + 2\beta)\Gamma_s\left(\frac{\partial^2 h_0}{\partial \tau^2} - \frac{\partial}{\partial \tau}(|\nabla h_0|^2)\right) - (k_E + \beta)\nabla^2 h_0 \\ &+ ((1 - k_E)\mu_{TS} + (k_E + 2\beta)\Gamma_s)\left(\frac{\partial h_0}{\partial \tau} - \frac{1}{2}|\nabla h_0|^2\right)\nabla^2 h_0 - (1 + \beta)\Gamma_s(\nabla^2 h_0)^2 - \frac{\mu_{TS}\beta(2 + k_E + 3\beta)}{8(1 + \beta)}|\nabla h_0|^4 \\ &+ (1 + 2k_E + 4\beta)\Gamma_s\nabla^2\left(\frac{\partial h_0}{\partial \tau}\right) - (1 + k_E + 2\beta)\Gamma_s\nabla^4 h_0 - \left(k_E + \frac{3}{2}\beta\right)\Gamma_s\nabla^2(|\nabla h_0|^2). \end{aligned} \quad (88)$$

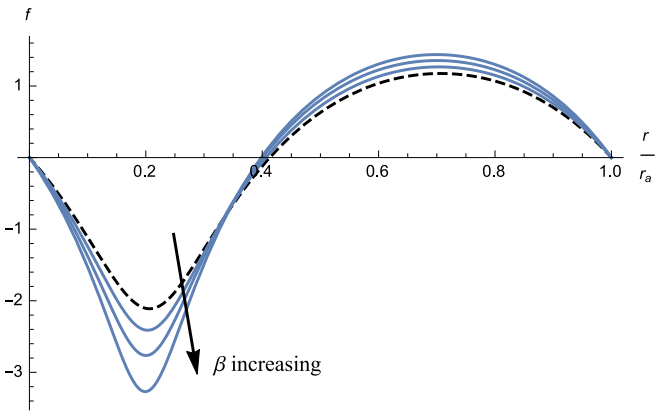

FIG. 6. Steady deflection of the solid-liquid interface in one horizontal dimension for various values of β, when $\mu_T = \mu_{TS}$ and $\Gamma_s - \Gamma = \epsilon \ll 1$. The solution for $\beta = 0$ obtained by Brattkus and Davis [4] is shown as a dashed curve. The horizontal axis is normalized by the critical wavelength r_a.

This evolution equation reduces to the one obtained by Brattkus and Davis [4] in the case of interfacial equilibrium ($\beta = 0, \mu_{TS} = 0$). A direct comparison against the equilibrium results of Brattkus and Davis [4] is shown in Fig. 6, where disequilibrium effects are seen to favor deep-rooted solutions.

VI. NONLINEAR OSCILLATORY GROWTH—REGIME II

The other absolute stability boundary involves attachment kinetics, which acts to suppress oscillatory instabilities. This branch is present only in disequilibrium ($\beta \neq 0$). The appropriate scaling is given by

$$\mu_T = \mu_{TS} - \epsilon^2, \quad \alpha = \epsilon\bar{\alpha}, \qquad \sigma = \epsilon\bar{\sigma}, \quad \mathcal{M}^{-1} = \epsilon^2\bar{\mathcal{M}}^{-1}, \tag{89a–d}$$

under which, the dispersion relation reduces to

$$\bar{\mathcal{M}}^{-1} = -\bar{\sigma}^2\Gamma_s\frac{(2\beta + k_E)}{\beta + k_E} + \bar{\alpha}^2(\Gamma_s - \Gamma). \tag{90}$$

We use the transformation

$$\tau = \epsilon t, \quad (\xi, \eta) = \epsilon^{1/2}(x, y), \quad \zeta = z - h, \tag{91a–c}$$

under which, the rescaled governing equations are given by

$$\epsilon(C_\tau - C_\zeta h_\tau) = \epsilon^2(C_{\zeta\zeta}|\nabla h|^2 - 2\nabla h\cdot\nabla C_\zeta - C_\zeta\nabla^2 h + \nabla^2 C) + C_\zeta + C_{\zeta\zeta}, \tag{92}$$

for $\zeta > 0$,

$$h\epsilon^2\bar{\mathcal{M}}^{-1} + \gamma = 2\Gamma\bar{H} - \bar{V}_n(\mu_{TS} - \epsilon^2) - \frac{1}{k_E - 1} + m\left(C + \frac{1}{k_E - 1}\right), \tag{93}$$

and

$$\bar{V}_n\left(C(1-k) - \frac{1}{\beta\bar{V}_n + 1}\right) = [\epsilon^2(\nabla C - C_\zeta\nabla h)\nabla h - C_\zeta][\epsilon^2|\nabla h|^2 + 1]^{-1/2}, \tag{94}$$

at $\zeta = 0$, and the decay condition

$$C \to \infty \quad \text{as} \quad \zeta \to \infty. \tag{95}$$

The normal velocity rescales to

$$\bar{V}_n = \frac{\epsilon h_\tau + 1}{\sqrt{\epsilon^2|\nabla h|^2 + 1}}, \tag{96}$$

and the rescaled mean curvature is given by

$$2\bar{H} = \left[\epsilon^2 h_{\xi\xi}\left(\epsilon^2 h_\eta^2 + 1\right) - 2\epsilon^4 h_\eta h_\xi h_{\xi\eta} + \epsilon^2 h_{\eta\eta}\left(\epsilon^2 h_\xi^2 + 1\right)\right][\epsilon^2|\nabla h|^2 + 1]^{-3/2}. \tag{97}$$

We seek solutions in powers of ϵ as follows:

$$C = C_0 + \epsilon C_1 + \epsilon^2 C_2 + \cdots, \qquad h = h_0 + \epsilon h_1 + \epsilon^2 h_2 + \cdots. \tag{98a,b}$$

Expansions for the normal velocity and mean curvature are given by

$$\bar{V}_n = V_0 + V_1\epsilon + V_2\epsilon^2 + \cdots, \tag{99}$$

$$2\bar{H} = 2H_1\epsilon + 2H_2\epsilon^2 + \cdots, \tag{100}$$

where

$$V_0 = 1, \quad V_1 = h_{0\tau}, \qquad V_2 = h_{1\tau} - \tfrac{1}{2}|\nabla h_0|^2, \tag{101a–c}$$

and

$$2H_1 = 0, \quad 2H_2 = \nabla^2 h_0. \tag{102a,b}$$

A. Zeroth order

At zeroth order in ϵ, the problem becomes

$$C_{0\zeta} + C_{0\zeta\zeta} = 0 \tag{103}$$

for $\zeta > 0$,

$$\gamma_0 = C_0 m_0 + \frac{m_0}{k_E - 1} - \frac{1}{k_E - 1} - \mu_{TS} \tag{104}$$

at $\zeta = 0$, where γ_0 is determined by

$$\gamma = \gamma_0 + \epsilon^2\gamma_2, \tag{105}$$

that is,

$$\gamma_0 = \frac{\beta}{(1 - k_E)(\beta + k_E)} - \frac{k_E\mathcal{L}}{(k_E - 1)^2} - \mu_{TS}, \qquad \gamma_2 = 1, \tag{106a,b}$$

and the remaining two boundary conditions as before. The solution is given by

$$C_0 = 1 - \delta e^{-\zeta}. \tag{107}$$

B. First order

At first order in ϵ, the problem becomes

$$C_{1\zeta} + C_{1\zeta\zeta} = -\delta e^{-\zeta} h_{0,\tau}, \tag{108}$$

for $\zeta > 0$,

$$2\Gamma \bar{H}_1 + C_1 m_0 + C_0 m_1 + \frac{m_1}{k_E - 1} - V_1 \mu_{TS} = 0, \tag{109}$$

and

$$-C_{1\zeta} = -V_1 \left(C_0 (k_0 - 1) + \frac{1}{(\beta + 1)^2} \right) + C_1 (1 - k_0) - C_0 k_1, \tag{110}$$

at $\zeta = 0$, as well as the usual decay condition. The solution is given by

$$C_1 = \left(\delta\zeta + \frac{\beta k_E}{(\beta + k_E)^2} \right) h_{0\tau} e^{-\zeta}. \tag{111}$$

C. Second order

At second order in ϵ, the problem reduces to

$$C_{2\zeta} + C_{2\zeta\zeta} = e^{-\zeta} \left[\delta \nabla^2 h_0 + \delta |\nabla h_0|^2 - \delta h_{1\tau} + h_{0\tau}^2 \left(\delta\zeta - \delta + \frac{\beta k_E}{(\beta + k_E)^2} \right) + h_{0\tau\tau} \left(\delta\zeta + \frac{\beta k_E}{(\beta + k_E)^2} \right) \right], \tag{112}$$

for $\zeta > 0$,

$$\frac{h_0}{\bar{\mathcal{M}}} = 2\Gamma \bar{H}_2 + m_2 \left(C_0 + \frac{1}{k_E - 1} \right) + C_2 m_0 + C_1 m_1 - V_2 \mu_{\mathrm{TS}}, \tag{113}$$

and

$$-C_{2,\zeta} = h_{0,\tau} \left(-\frac{\beta k_1 k_E}{(\beta + k_E)^2} - \frac{\beta (k_0 - 1) k_E V_1}{(\beta + k_E)^2} \right) + C_2 (1 - k_0) + (\delta - 1) k_2 + \frac{1}{2} \delta |\nabla h_0|^2 - \frac{V_2 (1 - (\beta + 1)^2 (\delta - 1)(k_0 - 1))}{(\beta + 1)^2} + (\delta - 1) k_1 V_1 + \frac{\beta V_1^2}{(\beta + 1)^3}, \tag{114}$$

at $\zeta = 0$, and

$$C_2 \to 0 \quad \text{as} \quad \zeta \to \infty. \tag{115}$$

Solutions exist only when the amplitude h_0 obeys the evolution equation

$$h_0 \bar{\mathcal{M}}^{-1} = -\frac{k_E \beta^2 (2 + k_E + 3\beta)}{2(1 + \beta)^2 (k_E + \beta)^3} \left(\frac{\partial h_0}{\partial \tau} \right)^2 - \Gamma_s \frac{k_E + 2\beta}{k_E + \beta} \left(\frac{\partial^2 h_0}{\partial \tau^2} \right) + (\Gamma - \Gamma_s) \nabla^2 h_0. \tag{116}$$

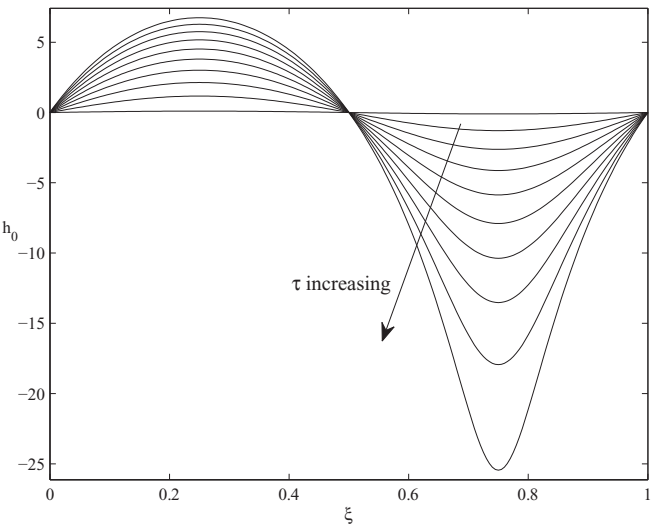

FIG. 7. The time-dependent position of the solid-liquid interface near the oscillatory absolute stability limit for $\beta = 0.5$ for several points in time, normalized by the wavelength. The solutions were obtained by numerically solving the time- and space-dependent evolution equation corresponding to the oscillatory absolute stability limit.

The steady, one-dimensional version of this equation reduces to

$$h_0 = -\bar{\mathcal{M}} (\Gamma_s - \Gamma) h_0'', \tag{117}$$

which has sinusoidal solutions of wavelength $2\pi/\sqrt{\bar{\mathcal{M}}(\Gamma_s - \Gamma)}$ for $\Gamma < \Gamma_s$. For $\Gamma > \Gamma_s$, cellular instabilities are completely suppressed and no periodic solutions exist.

The time-dependence introduces nonlinearity into the problem; as time progresses nonlinear effects become significant. Numerical solutions to the time-dependent partial differential equation for the progression of the deflection of the solid-liquid interface are shown in Fig. 7, where this effect is clearly seen. Strong asymmetries are seen to develop with time between the root and tip regions. The troughs sharply deepen with time.

This behavior can be understood by considering the spatially uniform version of the oscillatory evolution equation. Rescaling as

$$h_0 = h_s f(\mathscr{T}), \quad \mathscr{T} = T_s \tau, \tag{118a,b}$$

where

$$h_s = \frac{2(\beta + 1)(2\beta + k_E)\Gamma_s}{\beta(3\beta + k_E + 2)\mu_{\mathrm{TS}}}, \qquad T_s = \left(\frac{\beta + k_E}{(k_E + 2\beta)\bar{\mathcal{M}}\Gamma_s} \right)^{1/2}, \tag{119a,b}$$

leads to

$$\frac{d^2 f}{d\mathscr{T}^2} + \left(\frac{df}{d\mathscr{T}} \right)^2 + f = 0. \tag{120}$$

As it is always positive, the nonlinear term increases the amplitude of the oscillations for $f' < 0$ and decreases it for $f' > 0$. Solutions, therefore, sharpen near troughs. This is reflected in the time- and space-dependent solutions of

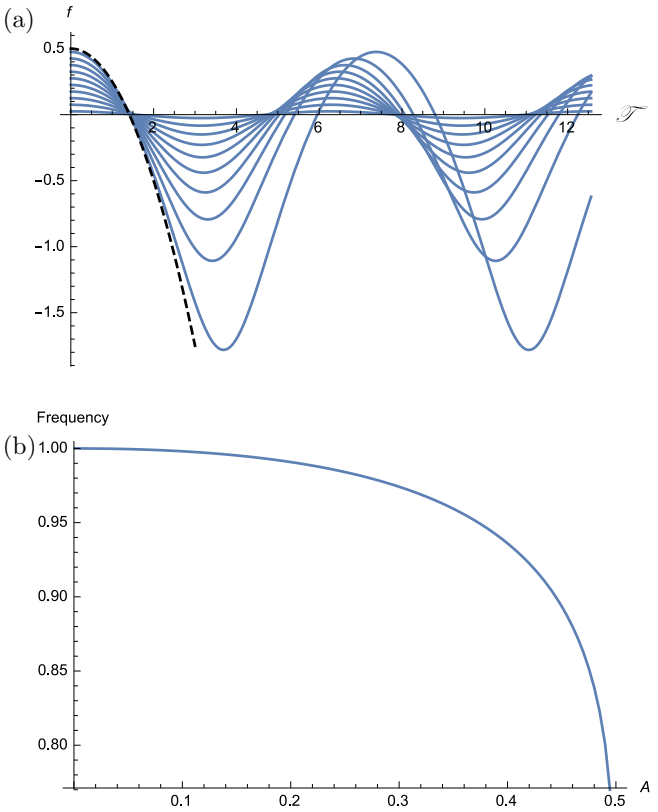

FIG. 8. (a) Solutions to Eq. (120) for varying values of A. The limiting solution for $A = 0.5$ is shown as a dashed curve. The associated frequencies as a function of A are shown in (b).

the full oscillatory evolution equation. Amplitudes near the troughs grow faster than near the peaks, leading to the strong asymmetry that develops with time.

Writing $u = f, v = df/d\mathscr{T}$, we note that Eq. (120) reduces to the simple form

$$\left(\frac{1}{2}\frac{d}{du} + 1\right)v^2 + u = 0. \tag{121}$$

Integrating once and reverting to the original variables gives the first order differential equation

$$\left(\frac{df}{d\mathscr{T}}\right)^2 = \left(A - \frac{1}{2}\right)e^{2(A-f)} - \left(f - \frac{1}{2}\right), \tag{122}$$

where A is a constant.

The system (120) has one equilibrium point, $f = 0$, which is marginally stable. Small displacements lead to oscillatory motion. Figure 8(a) shows solutions to Eq. (120) subject to the initial conditions $f(0) = A, f'(0) = 0$, for varying values of A. The frequency of the oscillations is amplitude dependent. Larger amplitudes lead to deeper roots and smaller frequencies as seen in Fig. 8(b). Small amplitudes lead to sinusoidal disturbances of period 2π. Solutions are periodic for $A < 0.5$, non-periodic for $A \geqslant 0.5$ and converge towards the limiting solution $f(\mathscr{T}) = 1/2 - \mathscr{T}^2/4$ (shown as a dashed curve in Fig. 8(a)) as $A \to 0.5$. This can be used in practice to tune the appearance of bands by tuning the initial system to a certain amplitude. Then, periodic bands will persist, with a size specified by the initial amplitude of the disturbance. Sample

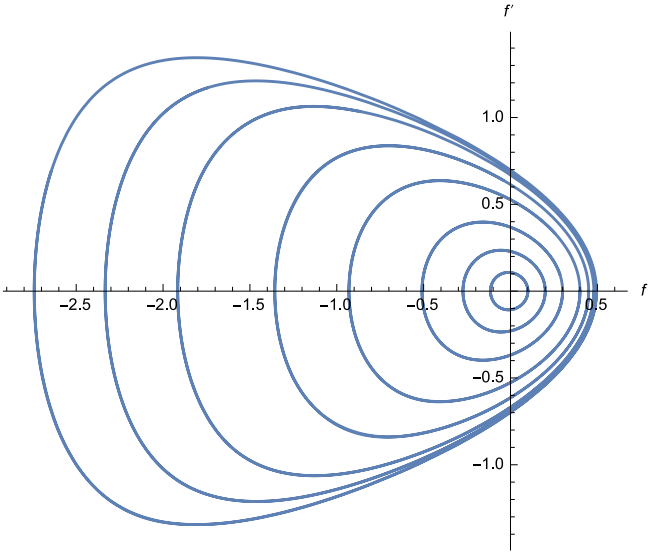

FIG. 9. Phase diagram for uniform oscillations for varying values of A.

phase-plane trajectories are shown in Fig. 9. Small amplitude oscillations correspond to circular trajectories centered at the origin in the phase diagram. On the other hand, large amplitude oscillations are no longer well approximated by linearized theory and favor deepening troughs.

The value of $\bar{\mathcal{M}}$ influences only the period of the oscillations, as seen by the scaling (123b). The period increases with increasing $\bar{\mathcal{M}}$. The value of $\bar{\mathcal{M}}$ does not affect the critical amplitude, which depends only on β and k_E through the scaling (123a) for h_s, shown in Fig. 10. The critical amplitude is smallest for $\beta = \mathcal{O}(1)$, and becomes large for small and large β. Non-periodic behavior is therefore most likely to occur for $\beta = \mathcal{O}(1)$. In contrast, in the equilibrium limit ($\beta = 0$), the critical amplitude is infinite, which corresponds to periodic behavior for all amplitudes. More precisely, if we rescale to an appropriate form for small β as

$$h_0 = \bar{h}_s \bar{f}(\mathscr{T}), \quad \mathscr{T} = T_s \tau, \tag{123a,b}$$

where

$$\bar{h}_s = \beta^2 h_s, \tag{124}$$

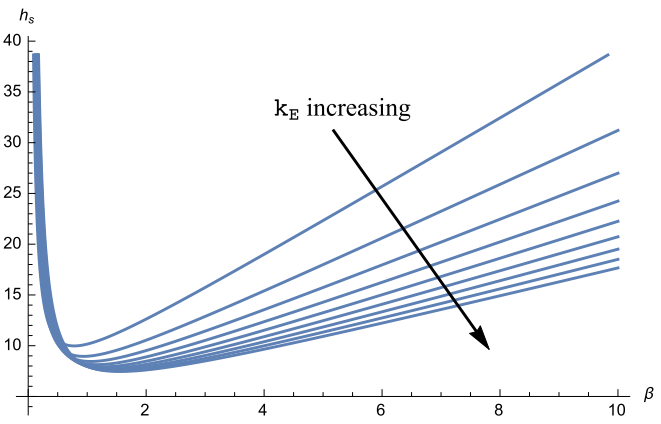

FIG. 10. h_s as a function of β for various values of k_E.

then $\bar{h}_s = \mathcal{O}(1)$ as $\beta \to 0$ and the spatially uniform version of the oscillatory evolution equation becomes

$$\frac{d^2\bar{f}}{d\mathscr{T}^2} + \left(\beta\frac{d\bar{f}}{d\mathscr{T}}\right)^2 + \bar{f} = 0. \tag{125}$$

In the limit $\beta = 0$, this equation yields periodic solutions with unit angular frequency, for all amplitudes as expected.

VII. A DISTINGUISHED LIMIT—REGIME III

A distinguished limit arises in which both $\Gamma_s - \Gamma$ and $\mu_{TS} - \mu_T$ are small. The same scalings as in Sec. V B are used, except that $\mu_T = \mu_{TS} - \epsilon\nu$ and $\Gamma = \Gamma_s - \epsilon\rho$, where $\nu, \rho = \mathcal{O}(1)$ as $\epsilon \to 0$, in this scenario. Explicitly,

$$\Gamma = \Gamma_s - \epsilon\rho, \quad \alpha = \epsilon^{1/2}\bar{\alpha}, \quad \sigma = \epsilon\bar{\sigma},$$
$$\mathcal{M}^{-1} = \epsilon^2\bar{\mathcal{M}}^{-1}, \quad \mu_T = \mu_{TS} - \epsilon\nu, \tag{126a–e}$$

under which, the dispersion relation becomes

$$\bar{\mathcal{M}}^{-1} = \bar{\alpha}^2\bar{\sigma}\left(\frac{2k_E - 1}{\beta + k_E} - 4\right)\Gamma_s + \rho\bar{\alpha}^2 + \bar{\alpha}^4\left(\frac{k_E - 1}{\beta + k_E} - 2\right)\Gamma_s + \bar{\sigma}^2\left(\frac{k_E}{\beta + k_E} - 2\right)\Gamma_s + \bar{\sigma}\nu, \tag{127}$$

at leading order. The governing equations remain unchanged except for the boundary condition (8), which becomes

$$\frac{h\epsilon^2}{\bar{\mathcal{M}}} + \gamma_0 + \gamma_1\epsilon = 2\bar{H}(\Gamma_s - \epsilon\rho) - \bar{V}_n(\mu_{TS} - \epsilon\nu) + m\left(C + \frac{1}{k_E - 1}\right) - \frac{1}{k_E - 1}, \tag{128}$$

where γ_0 remains as before but $\gamma_1 = \nu$. The difference occurs at second order in ϵ. The boundary condition reduces to

$$h_0\bar{\mathcal{M}}^{-1} = 2\bar{H}_2\Gamma_s - 2\rho\bar{H}_1 + C_2 m_0 + C_1 m_1 + C_0 m_2 + \frac{m_2}{k_E - 1} - V_2\mu_{TS} + V_1\nu. \tag{129}$$

Following the details laid out in Sec. V B, we find that the solid-liquid interface must satisfy the following evolution equation:

$$\begin{aligned} h_0\bar{\mathcal{M}}^{-1}(k_E + \beta) = {} & -(1+\beta)\Gamma_s\nabla h_0\cdot\nabla(\nabla^2 h_0) - \left(\frac{1}{2}k_E + \beta\right)\Gamma_s\nabla h_0\cdot\nabla(|\nabla h_0|^2) + \frac{\mu_{TS}\beta(2 + k_E + 3\beta)}{2(1+\beta)}\frac{\partial h_0}{\partial\tau}|\nabla h_0|^2 \\ & - \frac{\mu_{TS}\beta(2 + k_E + 3\beta)}{2(1+\beta)}\left(\frac{\partial h_0}{\partial\tau}\right)^2 - (k_E + 2\beta)\Gamma_s\left(\frac{\partial^2 h_0}{\partial\tau^2} - \frac{\partial}{\partial\tau}(|\nabla h_0|^2)\right) + \nu(\beta + k_E)\left(\frac{\partial h_0}{\partial\tau} - \frac{1}{2}|\nabla h_0|^2\right) \\ & + ((1 - k_E)\mu_{TS} + (k_E + 2\beta)\Gamma_s)\left(\frac{\partial h_0}{\partial\tau} - \frac{1}{2}|\nabla h_0|^2\right)\nabla^2 h_0 - (1+\beta)\Gamma_s(\nabla^2 h_0)^2 - \frac{\mu_{TS}\beta(2+k_E+3\beta)}{8(1+\beta)}|\nabla h_0|^4 \\ & + (1 + 2k_E + 4\beta)\Gamma_s\nabla^2\left(\frac{\partial h_0}{\partial\tau}\right) - (1 + k_E + 2\beta)\Gamma_s\nabla^4 h_0 - \left(k_E + \frac{3}{2}\beta\right)\Gamma_s\nabla^2(|\nabla h_0|^2) - (k_E + \beta)\nabla^2 h_0. \end{aligned} \tag{130}$$

This evolution equation reduces to the one presented in Sec. V B in the limit $\nu \to 0$.

The steady, one-dimensional version of this equation reduces to

$$\begin{aligned} & (\beta + k_E)\left(h_0\bar{\mathcal{M}}^{-1} + \frac{\nu}{2}(h_0')^2 + \rho h_0''\right) \\ & + (2\beta + k_E + 1)\Gamma_s h_0^{(4)} \\ & + \frac{1}{2}(3(2\beta + k_E)\Gamma_s + (1 - k_E)\mu_{TS})(h_0')^2 h_0'' \\ & + \frac{\beta(3\beta + k_E + 2)}{8(\beta + 1)}\mu_{TS}(h_0')^4 \\ & + (4\beta + 2k_E + 1)\Gamma_s(h_0^{(3)}h_0' + (h_0'')^2) = 0. \end{aligned} \tag{131}$$

We adopt the scalings

$$f = \frac{1}{2k_E + 1}H_0, \quad r = \frac{k_E^{3/2}}{2k_E + 1}\xi, \tag{132a,b}$$

and transformation

$$\bar{\nu} = \frac{1}{1 + 2k_E}, \quad \bar{\mu}^{-1} = \frac{(2k_E + 1)^2}{k_E^3}\bar{\mathcal{M}}^{-1}, \tag{133a,b}$$

used by Brattkus and Davis [4]. Equation (131) then becomes

$$\begin{aligned} & \frac{f}{\bar{\mu}} + R\cos\theta f_{rr} + \bar{\Gamma}_S(f_{rr}^2 + f_r f_{rrr}) + \frac{R\sin\theta}{2\bar{\nu}}f_r^2 - \bar{\mu}_{TS}f_r^4 \\ & + \frac{\bar{\nu}(4\beta\bar{\nu} + \bar{\nu} + 1)}{8\beta\bar{\nu} + 2}\bar{\Gamma}_S f_{rrrr} + \left(\frac{3}{4}\left(\frac{1}{\bar{\nu}} - \frac{1}{4\beta\bar{\nu} + 1}\right)\bar{\Gamma}_S \right. \\ & \left. - \frac{4\bar{\nu}(\beta + 1)(3\bar{\nu} - 1)}{\beta((6\beta + 3)\bar{\nu} + 1)}\bar{\mu}_{TS}\right)f_r^2 f_{rr} = 0, \end{aligned} \tag{134}$$

where

$$\bar{\Gamma}_S = \frac{k_E^3(4\beta + 2k_E + 1)\Gamma_s}{(2k_E + 1)(\beta + k_E)},$$
$$\bar{\mu}_{TS} = -\frac{\beta k_E^3(2k_E + 1)(3\beta + k_E + 2)\mu_{TS}}{8(\beta + 1)(\beta + k_E)}, \tag{135a,b}$$

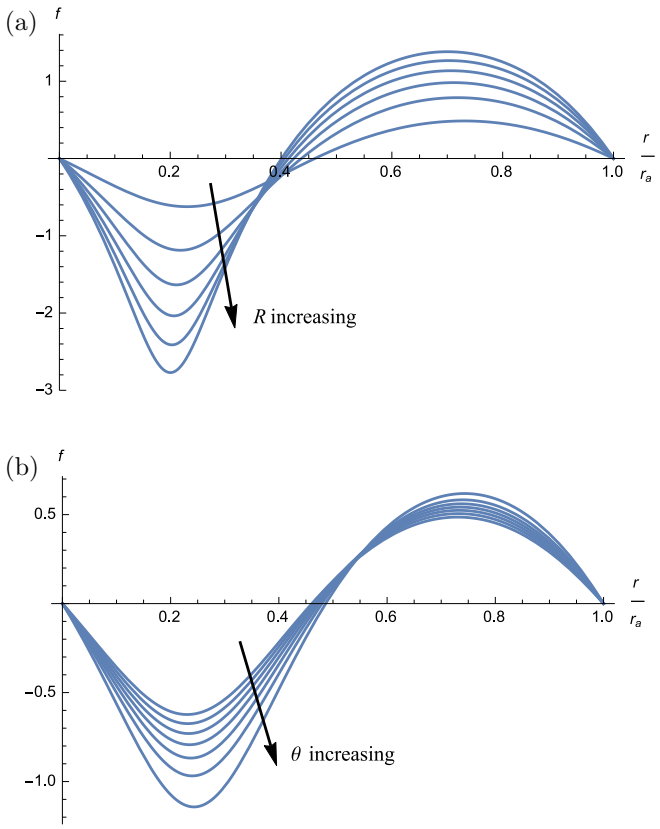

FIG. 11. Steady deflection of the solid-liquid interface in one horizontal dimension for various values of (a) R and (b) θ in the distinguished limit, in which both $\Gamma_s - \Gamma$ and $\mu_{TS} - \mu_T$ are small. The horizontal axis is normalized by the critical wavelength.

and

$$R = \sqrt{\rho^2 + \nu^2}, \quad \theta = \tan^{-1}\left(\frac{\nu}{\rho}\right) \qquad (136a,b)$$

(see Fig. 1). Its solution is shown in Figs. 6, 11, and 12 for various values of β, R, θ, and $\bar{\mu}$. Here, we have imposed periodic boundary conditions using the critical wavelength $r = r_a$. Increasing β, R, θ, and $\bar{\mu}$ is seen to give deeper rooted solutions.

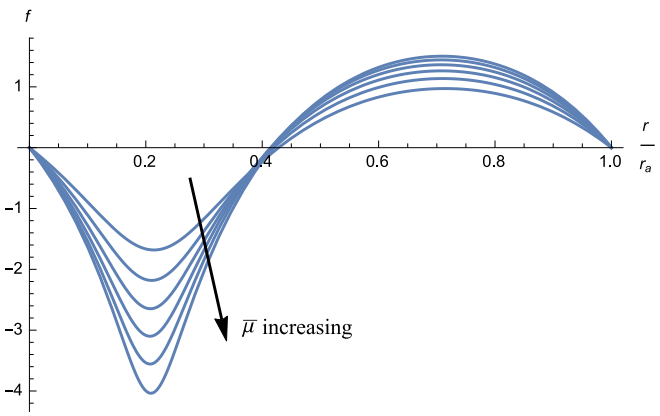

FIG. 12. Steady deflection of the solid-liquid interface in one horizontal dimension for various values of $\bar{\mu}$ in the distinguished limit, in which both $\Gamma_s - \Gamma$ and $\mu_{TS} - \mu_T$ are small. The horizontal axis is normalized by the wavelength.

VIII. CONCLUSIONS

We have conducted long-wave nonlinear stability analyses near two absolute stability boundaries in five scenarios that appear depending on the surface energy and attachment kinetics. In each of these scenarios, we derive corresponding nonlinear evolution equations that describe the large deformations of solid-liquid interfaces at disequilibrium and solve them numerically for various disequilibrium conditions. The two absolute stability boundaries involve the appearance of either cellular or oscillatory modes.

An interesting aspect that we observe in our numerical solutions stems from the appearance of the oscillatory absolute stability boundary and its intricate interaction with the cellular dynamics. The coupling between these two branches lead to a breadth of different scenarios. A common theme between all of these is the sharpening of asymmetries between peaks and troughs for larger disequilibrium and larger morphological numbers, characterized by deepening troughs.

The first regime that we study, Regime I, involves the appearance of cellular modes near the cellular absolute stability boundary $\Gamma = \Gamma_s$. The dynamics in this regime are dominated by the departure from critical attachment kinetics. In particular, the dynamics depend on whether or not the oscillatory modes are present.

We have also examined nonlinear dynamics near the oscillatory absolute stability boundary. This region is referred to as Regime II. We find that both oscillations and monotonic growth may emerge and that there is a single combination of parameters as well as the value of the initial amplitude that determines which one of these occurs. Interestingly, the asymmetries near the oscillatory absolute stability boundary rapidly sharpen with time and feature sharply deepening troughs.

Finally, Regime III, involves states close to both absolute stability boundaries, and may admit both cellular and oscillatory growth. For this regime, we first derive an evolution equation when $\mu_T = \mu_{TS}$ and $\Gamma - \Gamma_s$ small, and then generalise it to a distinguished limit in which both $\mu_T - \mu_{TS}$ and $\Gamma - \Gamma_s$ are nonzero and small. This regime is one in which the dynamics are qualitatively similar to those reported by Brattkus and Davis [4] and our nonlinear evolution equations in these two scenarios reduce to that of the equilibrium study of [4] exactly in the limit of zero disequilibrium and zero attachment kinetics. We find that the effects of disequilibrium introduce stronger asymmetries in the disturbances, including deepening roots.

Physically, the effects of disequilibrium and attachment kinetics may be seen to give rise to spatial structure and speed up the transition to dendritic growth. All of the regimes depicted in Fig. 1 are characterized by a sharpening of the disturbances and the appearance of time-dependence, which is an expected feature of the solidification process. The dynamics depend on the region of parameter space and the interplay between the two modes of instability. The cellular modes of

Regime *I* sharpen and spatial structure emerges in the solute bands of Regime *II*. A combination of these is observed for the disturbances of Regime *III*, close to both absolute stability boundaries.

ACKNOWLEDGMENTS

This work is supported by the National Institute of Standards and Technology (Grant No. 70NANB14H012) as part of the Center for Hierarchical Material Design (CHiMaD).

[1] W. W. Mullins and R. F. Sekerka, J. Appl. Phys. **35**, 444 (1964).
[2] S. R. Coriell and G. B. McFadden, in *Handbook of Crystal Growth*, Vol. 1, edited by D. T. J. Hurle (Elsevier, Amsterdam, 1993), pp. 785–858.
[3] D. J. Wollkind and L. A. Segel, Philos. Trans. R. Soc. London Ser. A **268**, 351 (1970).
[4] K. Brattkus and S. H. Davis, Phys. Rev. B **38**, 11452 (1988).
[5] J. C. Baker and J. W. Cahn, *Solidification* (American Society of Metals, Metals Park, OH, 1971), p. 23.
[6] K. Jackson, G. Gilmer, and H. Leamy, in *Laser and Electron Beam Processing of Materials*, edited by C. White and P. Peercy (Academic Press, New York, 1980), pp. 104–110.
[7] M. J. Aziz, J. Appl. Phys. **53**, 1158 (1982).
[8] W. J. Boettinger and J. H. Perepezko, in *Rapidly Solidified Crystalline Alloys, Proc. TMS-AIME Northeast Regional Meeting, Morriston, N.J.*, edited by S. K. Das, B. H. Kear, and C. M. Adam (The Metallurgical Society, Warrendale, PA, 1985), p. 21.
[9] W. J. Boettinger and S. R. Coriell, in *Rapid Solidification Materials and Technologies*, edited by P. R. Sahm, H. Jones, and C. M. Adam (NATO, 1986).
[10] W. Kurz and D. J. Fisher, *Fundamentals of Solidification*, 3rd ed. (Trans Tech Publications, Switzerland, 1989).
[11] S. R. Coriell and R. F. Sekerka, J. Cryst. Growth **61**, 499 (1983).
[12] G. J. Merchant and S. H. Davis, Acta Metall. Mater. **38**, 2683 (1990).
[13] R. J. Braun and S. H. Davis, J. Cryst. Growth **112**, 670 (1991).
[14] G. J. Merchant, R. J. Braun, K. Brattkus, and S. H. Davis, SIAM J. Appl. Math. **52**, 1279 (1992).
[15] R. J. Braun, G. J. Merchant, and S. H. Davis, Phys. Rev. B **45**, 7002 (1992).
[16] S. H. Davis, *Theory of Solidification* (Cambridge University Press, Cambridge, 2001).